Nitrogen Kinetic Isotope Effects of Nitrification by the Complete Ammonia Oxidizer Nitrospira inopinata

Liu, Shurong; Jung, Man Young; Zhang, Shasha; Wagner, Michael; Daims, Holger; Wanek, Wolfgang

Published in:
mSphere

DOI (link to publication from Publisher):
10.1128/mSphere.00634-21

Publication date:
2021

Document Version
Publisher's PDF, also known as Version of record

AMERICAN SOCIETY FOR MICROBIOLOGY | mSphere®

RESEARCH ARTICLE

Nitrogen Kinetic Isotope Effects of Nitrification by the Complete Ammonia Oxidizer *Nitrospira inopinata*

Shurong Liu,[a,b,c] Man-Young Jung,[a,d,e] Shasha Zhang,[a] Michael Wagner,[a,b,f] Holger Daims,[a,b] Wolfgang Wanek[a,b]

[a]University of Vienna, Centre for Microbiology and Environmental Systems Science, Vienna, Austria
[b]University of Vienna, The Comammox Research Platform, Vienna, Austria
[c]Shenzhen Campus of Sun Yat-Sen University, School of Agriculture, Shenzhen, China
[d]Department of Biology Education, Jeju National University, Jeju, Republic of Korea
[e]Interdisciplinary Graduate Program in Advance Convergence Technology and Science, Jeju National University, Jeju, Republic of Korea
[f]Aalborg University, Department of Chemistry and Bioscience, Aalborg, Denmark

ABSTRACT Analysis of nitrogen isotope fractionation effects is useful for tracing biogeochemical nitrogen cycle processes. Nitrification can cause large nitrogen isotope effects through the enzymatic oxidation of ammonia (NH_3) via nitrite (NO_2^-) to nitrate (NO_3^-) ($^{15}\varepsilon_{NH4+\rightarrow NO2-}$ and $^{15}\varepsilon_{NO2-\rightarrow NO3-}$). The isotope effects of ammonia-oxidizing bacteria (AOB) and archaea (AOA) and of nitrite-oxidizing bacteria (NOB) have been analyzed previously. Here, we studied the nitrogen isotope effects of the complete ammonia oxidizer (comammox) *Nitrospira inopinata* that oxidizes NH_3 to NO_3^-. At high ammonium (NH_4^+) availability (1 mM) and pH between 6.5 and 8.5, its $^{15}\varepsilon_{NH4+\rightarrow NO2-}$ ranged from −33.1 to −27.1‰ based on substrate consumption (residual substrate isotopic composition) and −35.5 to −31.2‰ based on product formation (cumulative product isotopic composition), while the $^{15}\varepsilon_{NO2-\rightarrow NO3-}$ ranged from 6.5 to 11.1‰ based on substrate consumption. These values resemble isotope effects of AOB and AOA and of NOB in the genus *Nitrospira*, suggesting the absence of fundamental mechanistic differences between key enzymes for ammonia and nitrite oxidation in comammox and canonical nitrifiers. However, ambient pH and initial NH_4^+ concentrations influenced the isotope effects in *N. inopinata*. The $^{15}\varepsilon_{NH4+\rightarrow NO2-}$ based on product formation was smaller at pH 6.5 (−31.2‰) compared to pH 7.5 (−35.5‰) and pH 8.5 (−34.9‰), while $^{15}\varepsilon_{NO2-\rightarrow NO3-}$ was smaller at pH 8.5 (6.5‰) compared to pH 7.5 (8.8‰) and pH 6.5 (11.1‰). Isotopic fractionation via $^{15}\varepsilon_{NH4+\rightarrow NO2-}$ and $^{15}\varepsilon_{NO2-\rightarrow NO3-}$ was smaller at 0.1 mM NH_4^+ compared to 0.5 to 1.0 mM NH_4^+. Environmental factors, such as pH and NH_4^+ availability, therefore need to be considered when using isotope effects in ^{15}N isotope fractionation models of nitrification.

IMPORTANCE Nitrification is an important nitrogen cycle process in terrestrial and aquatic environments. The discovery of comammox has changed the view that canonical AOA, AOB, and NOB are the only chemolithoautotrophic organisms catalyzing nitrification. However, the contribution of comammox to nitrification in environmental and technical systems is far from being completely understood. This study revealed that, despite a phylogenetically distinct enzymatic repertoire for ammonia oxidation, nitrogen isotope effects of $^{15}\varepsilon_{NH4+\rightarrow NO2-}$ and $^{15}\varepsilon_{NO2-\rightarrow NO3-}$ in comammox do not differ significantly from those of canonical nitrifiers. Thus, nitrogen isotope effects are not suitable indicators to decipher the contribution of comammox to nitrification in environmental samples. Moreover, this is the first systematic study showing that the ambient pH and NH_4^+ concentration influence the isotope effects of nitrifiers. Hence, these key parameters should be considered in comparative analyses of isotope effects of nitrifiers across different growth conditions and environmental samples.

Editor Jorge L. M. Rodrigues, University of California, Davis

Address correspondence to Holger Daims, holger.daims@univie.ac.at.

The authors declare no conflict of interest.

Received 15 July 2021
Accepted 29 November 2021
Published 8 December 2021

KEYWORDS comammox, isotope fractionation, kinetic isotope effect, nitrification

Natural abundance isotope techniques have proven useful for studying nitrogen (N) transformation processes in aquatic and terrestrial ecosystems (1–3). Several process-oriented models that integrate isotope effects have been reported (4, 5). However, the successful integration of N isotopic composition into N cycle models requires the knowledge of the accurate isotope effects of each N transformation process. Until now, multiple N isotope effects have been reported based on soil and groundwater studies and for microbial isolates (3).

Nitrification represents a two-step N cycle process where ammonia (NH_3) is first oxidized to nitrite (NO_2^-) by ammonia-oxidizing bacteria (AOB) and archaea (AOA), followed by the oxidation of NO_2^- to nitrate (NO_3^-) by nitrite-oxidizing bacteria (NOB). Intriguingly, nitrification has shown much larger isotope effects than other N cycle processes, including biological N_2 fixation, mineral N uptake, ammonification, and denitrification (3). Isotope effects ($^{15}\varepsilon_{NH4+\rightarrow NO2-}$) for ammonia oxidation to NO_2^- have been determined in enriched and pure cultures of AOB and AOA (6–9). The AOB strain *Nitrosomonas europaea* exhibited an isotope effect of −38 to −32‰, whereas *Nitrosomonas marina*, *Nitrosomonas* sp. C-113a, and *Nitrosospira tenuis* showed smaller isotope effects in the range of −25 to −14‰ (6, 7). Measured isotope effects of AOA were in the same range as those of AOB, with a large variation of −21‰ ± 10‰ (8), regardless of whether the AOA had been cultured from marine or geothermal sources (9). The factors causing the large variations of the measured isotope effects in AOA and AOB have remained largely unknown. Possible causes include differences in the pH and in initial NH_4^+ concentrations between studies, amino acid substitutions in ammonia monooxygenase (AMO; the key enzyme for ammonia oxidation in AOB and AOA), and any isotope effect possibly involved in the subsequent oxidation of the AMO product hydroxylamine (NH_2OH) to NO_2^-, and with gaseous N losses via nitric oxide (NO) or nitrous oxide (N_2O) (7, 9).

Only a few studies have addressed isotopic fractionation during NO_2^- oxidation. The isotope effect of the key nitrite-oxidizing enzyme, nitrite oxidoreductase (NXR) ($^{15}\varepsilon_{NO2\rightarrow NO3-}$), became a focus of attention when the difference of $\delta^{15}N$ between NO_3^- and NO_2^- in marine samples turned out to be surprisingly large (10, 11). This was unexpected, because processes consuming NO_2^- (such as NO_2^- oxidation) or NO_3^- (denitrification) should increase the δ^{15} N residual NO_2^- and NO_3^-, respectively, and lead to a smaller offset in the $\delta^{15}N$ than observed. Hence, these results were taken as an indication for a process that actually decreased the $\delta^{15}NO_2^-$ relative to $\delta^{15}NO_3^-$ (12). Indeed, a subsequent study revealed an inverse isotope effect of NXR, where the substrate (NO_2^-) became more depleted in ^{15}N compared to the product (NO_3^-) in the marine NOB *Nitrococcus mobilis* (10). This contrasts with most other enzymatic processes of the N cycle, where the substrate becomes ^{15}N enriched and the product ^{15}N depleted. Three explanations for such inverse kinetic isotope effects were studied, i.e., equilibrium isotope effects between NO_2^- and nitrous acid before reaction, reaction reversibility at the enzyme level, and real inverse kinetic isotope fractionation (10). The inverse isotope effect of NXR most likely originates at the enzyme level, where larger force constants in the transition state explain the inverse kinetic isotope effect when stretching vibrational contributions dominate the kinetic isotope effect (13). Follow-up studies demonstrated inverse isotope effects of the NOB *Nitrococcus* and *Nitrobacter* to be similar and around 20.5‰, whereas the inverse isotope effects of the NOB *Nitrospira* and *Nitrospina* were less pronounced and close to 9.5‰ (11, 14), and those of anammox bacteria were larger with 30.1 to 45.3‰ (15). The cause for the quantitatively different isotope effects of $^{15}\varepsilon_{NO2\rightarrow NO3-}$ in the diverse NOB remained unclear. Possibly responsible factors include the orientation of the membrane-attached NXR toward either the cytoplasm or periplasm, kinetic differences among the known forms of NXR, and the reversibility of NO_2^- oxidation by this enzyme (i.e., its capability to also catalyze NO_3^- reduction) (14).

Complete ammonia oxidizers (comammox organisms), which oxidize NH_3 to NO_3^- on their own, were recently discovered in the genus *Nitrospira* (16, 17). Comammox

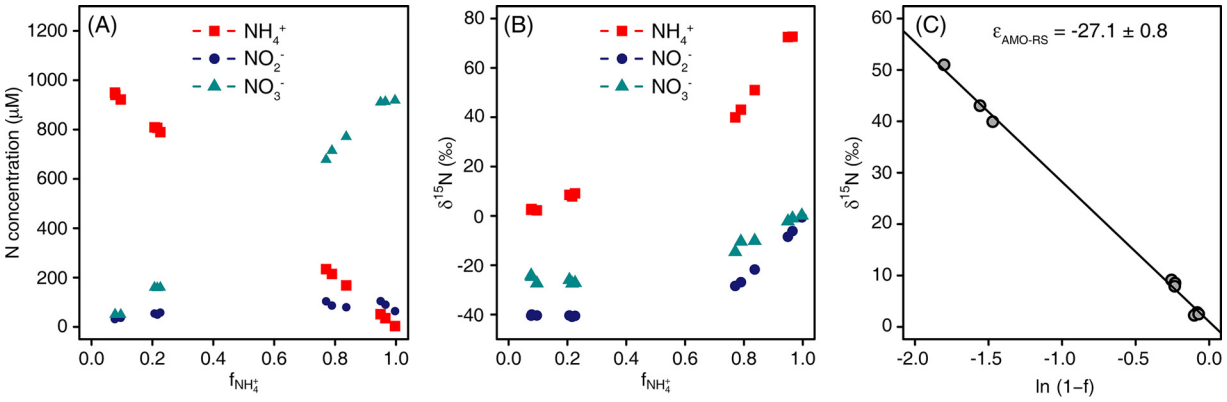

FIG 1 Kinetic isotope effect of *N. inopinata* cultivated in $CaCO_3$-buffered medium with 1 mM ammonium (NH_4^+) initial concentration. (A) Concentrations of NH_4^+, nitrite (NO_2^-), and nitrate (NO_3^-). (B) Isotopic signatures of NH_4^+, NO_2^-, and NO_3^-. (C) $^{15}\varepsilon_{NH4+\rightarrow NO2-}$ based on the residual substrate ($\varepsilon_{AMO\text{-}RS}$).

organisms are widespread in natural and engineered ecosystems (18). They possess a distinct form of AMO, which is phylogenetically moderately related to the AMO of betaproteobacterial AOB (16, 17). Generally, it is assumed that NH_3 and not NH_4^+ is the substrate for AMO in AOB, AOA, and comammox (19, 20). The only available comammox isolate, *Nitrospira inopinata*, has a very high substrate affinity for ammonia that exceeds the affinities of all characterized AOB and several AOA (21). Comammox bacteria share a highly similar NXR with canonical (only NO_2-oxidizing) *Nitrospira*, but the affinity of *N. inopinata* for NO_2^- is much lower than that reported for canonical *Nitrospira* (21, 22). The unique kinetic properties of comammox, and the distinct AMO, raise the question of whether NH_3 and NO_2^- oxidation by comammox might show comparable or different isotope effects than found in the canonical nitrifiers. So far, however, no isotope fractionation data from comammox have been available. In this study, we analyzed the N kinetic isotope effects of ammonia oxidation ($^{15}\varepsilon_{NH4+\rightarrow NO2-}$) and nitrite oxidation ($^{15}\varepsilon_{NO2-\rightarrow NO3-}$) of a pure culture of *N. inopinata*. In addition, we explored whether the isotope effect is influenced by selected environmental factors (medium pH and initial NH_4^+ concentration). The results provide important constraints for the interpretation of natural abundance stable isotope ratios for N compounds in systems where comammox *Nitrospira* are prevalent.

RESULTS

Experiment 1: ammonia oxidation with an initial concentration of 1 mM NH_4^+. Within 2 weeks of this incubation experiment, *N. inopinata* oxidized the initially provided 1 mM NH_4^+ to approximately 90% NO_3^- and 10% NO_2^- (Fig. 1A). A transient accumulation of NO_2^- was also observed in previous studies with *N. inopinata*, where the residual NO_2^- was finally converted to NO_3^- during prolonged incubations after NH_4^+ depletion (16, 21). The ratio of NH_4^+ consumption to NO_2^- plus NO_3^- formation was close to 1.0, indicating that ammonia was almost stoichiometrically oxidized to NO_2^- and NO_3^- (Fig. 1A). The initial $\delta^{15}N$ of NH_4^+ was −0.6‰. The $\delta^{15}N$ of NH_4^+ increased exponentially with incubation time, along with an increase of $\delta^{15}N$ of NO_2^- and NO_3^-. Moreover, the $\delta^{15}N$ of NO_2^- was depleted compared to the $\delta^{15}N$ of NH_4^+ and NO_3^- during the incubation (Fig. 1B). The $^{15}\varepsilon_{NH4+\rightarrow NO2-}$ was −27.1‰ ± 0.8‰ based on the residual substrate (equation 2, Fig. 1C, and Table 1) and −32.2‰ ± 1.4‰ based on the cumulative product (Table 1), which was in agreement with the $^{15}\varepsilon_{NH4+\rightarrow NO2-}$ (−38 to −14‰) of canonical AOB and AOA (7, 8). The $^{15}\varepsilon_{NO2-\rightarrow NO3-}$ was 7.6‰ ± 0.2‰ based on the residual substrate from the Solver model (Table 1), which was close to the canonical *Nitrospira* NOB (9‰) (11, 14).

Experiment 2: nitrite oxidation with an initial concentration of 1 mM NO_2^-. In a subsequent experiment, the $^{15}\varepsilon_{NO2-\rightarrow NO3-}$ was directly measured from a batch incubation with NO_2^- as a substrate. Since *N. inopinata* is unable to utilize NO_2^- as an N

TABLE 1 Modeled kinetic isotope effects (mean ± s.d., $n = 3$) of AMO and NXR of *Nitrospira inopinata*[a]

NH_4^+ (mM)	pH	NH_4^+/NO_2^- oxidation rate (μM/h)	NH_4^+ oxidation rate [μmol N (mg protein)$^{-1}$ h^{-1}]	$\varepsilon_{AMO\text{-}RS}$ (‰)	$\varepsilon_{AMO\text{-}CP}$ (‰)	$\varepsilon_{NXR\text{-}RS}$ (‰)
1	6.5	15.8 ± 2.6	V_{max} (12.8)	−30.1 ± 0.5	−31.2 ± 0.3	11.1 ± 0.6
1	7.5	18.6 ± 0.7	V_{max} (12.8)	−31.6 ± 0.5	−35.5 ± 0.2	8.8 ± 0.6
1	8.5	14.0 ± 1.7	V_{max} (12.8)	−33.1 ± 0.8	−34.9 ± 1.6	6.5 ± 1.0
0.1	8.2	5.8 ± 0.3[b]	2.1 ± 0.1	−19.7	−17.3	6.2
0.25	8.2	8.6 ± 0.4	3.1 ± 0.1	−21.1 ± 1.3	−21.2 ± 2.3	10.8 ± 1.1
0.5	8.2	10.7 ± 0.5	3.8 ± 0.2	−24.8 ± 0.2	−24.3 ± 1.9	10.5 ± 2.3
1	8.2	6.2 ± 0.4[c]		−27.1 ± 0.8	−32.2 ± 1.4	7.6 ± 0.2
1	8.2	39.5 ± 4.6				9.2 ± 0.5

[a]Modeled kinetic isotope effects (mean ± standard deviation, $n = 3$) of AMO and NXR of *Nitrospira inopinata* based on the Solver model at pH 6.5 to 8.5 with initial NH_4^+ concentrations of 0.1 to 1 mM.
[b]AOA/AOB medium buffered with $CaCO_3$ (pH around 8.2) was used for this batch experiment with 0.1, 0.25, and 0.5 mM NH_4^+.
[c]The batch experiment was performed with $CaCO_3$-buffered medium but with much less biomass.

source for assimilation (16), growth was not expected to occur during the incubation experiment with NO_2^-. Thus, we used an already highly concentrated cell suspension to analyze the $^{15}\varepsilon_{NO2^-\rightarrow NO3^-}$. Within 2 days of incubation, the initially provided 1 mM NO_2^- was almost stoichiometrically oxidized to NO_3^- (Fig. 2A). The ratio of NO_2^- oxidation to NO_3^- production was 1.03 ± 0.03. The initial $\delta^{15}N$ of NO_2^- was −25‰, and the $\delta^{15}N$ of both NO_2^- and NO_3^- decreased along with NO_2^- oxidation. In agreement with previous studies of canonical NOB (see introduction), the $\delta^{15}N$ of NO_2^- was depleted compared to the $\delta^{15}N$ of NO_3^- during NO_2^- oxidation (Fig. 2B). The calculated, inverse isotope effect of $^{15}\varepsilon_{NO2^-\rightarrow NO3^-}$ was 9.2‰ ± 0.5‰ based on the Rayleigh models for the residual substrate (Fig. 2C), which was similar with the above-mentioned $^{15}\varepsilon_{NO2^-\rightarrow NO3^-}$ (7.6‰ ± 0.2‰) calculated from the Solver model during NH_3 oxidation. Figure 2D shows the calculated $^{15}\varepsilon_{NO2^-\rightarrow NO3^-}$ based on the cumulative product.

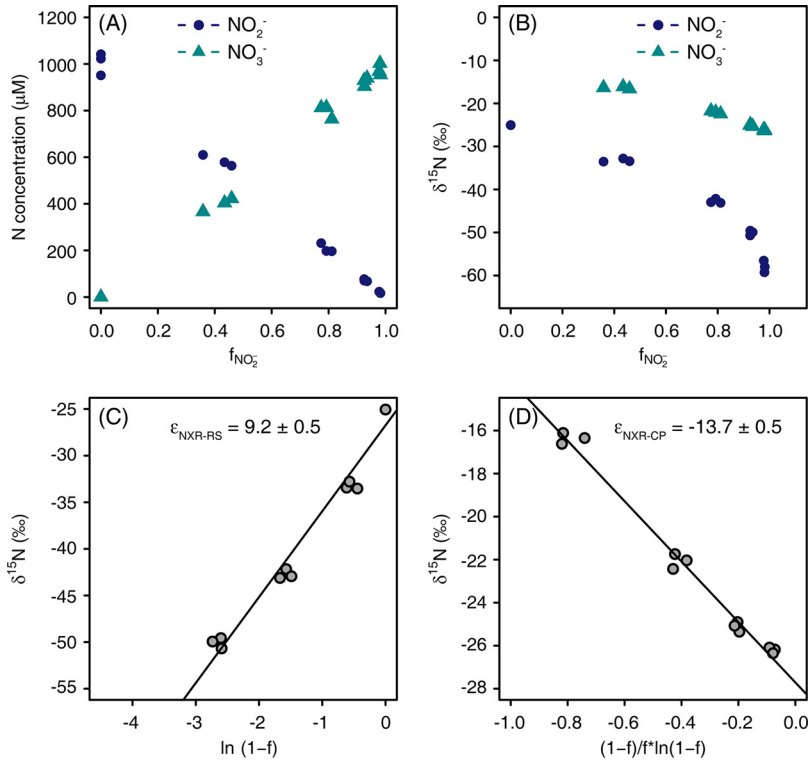

FIG 2 Kinetic isotope effect of *N. inopinata* cultivated in $CaCO_3$-buffered medium with 1 mM NO_2^- initial concentration. (A) Concentrations of NO_2^- and NO_3^-. (B) Isotopic signatures of NO_2^- and NO_3^-. (C and D) $^{15}\varepsilon_{NO2^-\rightarrow NO3^-}$ based on the residual substrate ($\varepsilon_{NXR\text{-}RS}$) (C) and cumulative product ($\varepsilon_{NXR\text{-}CP}$) (D).

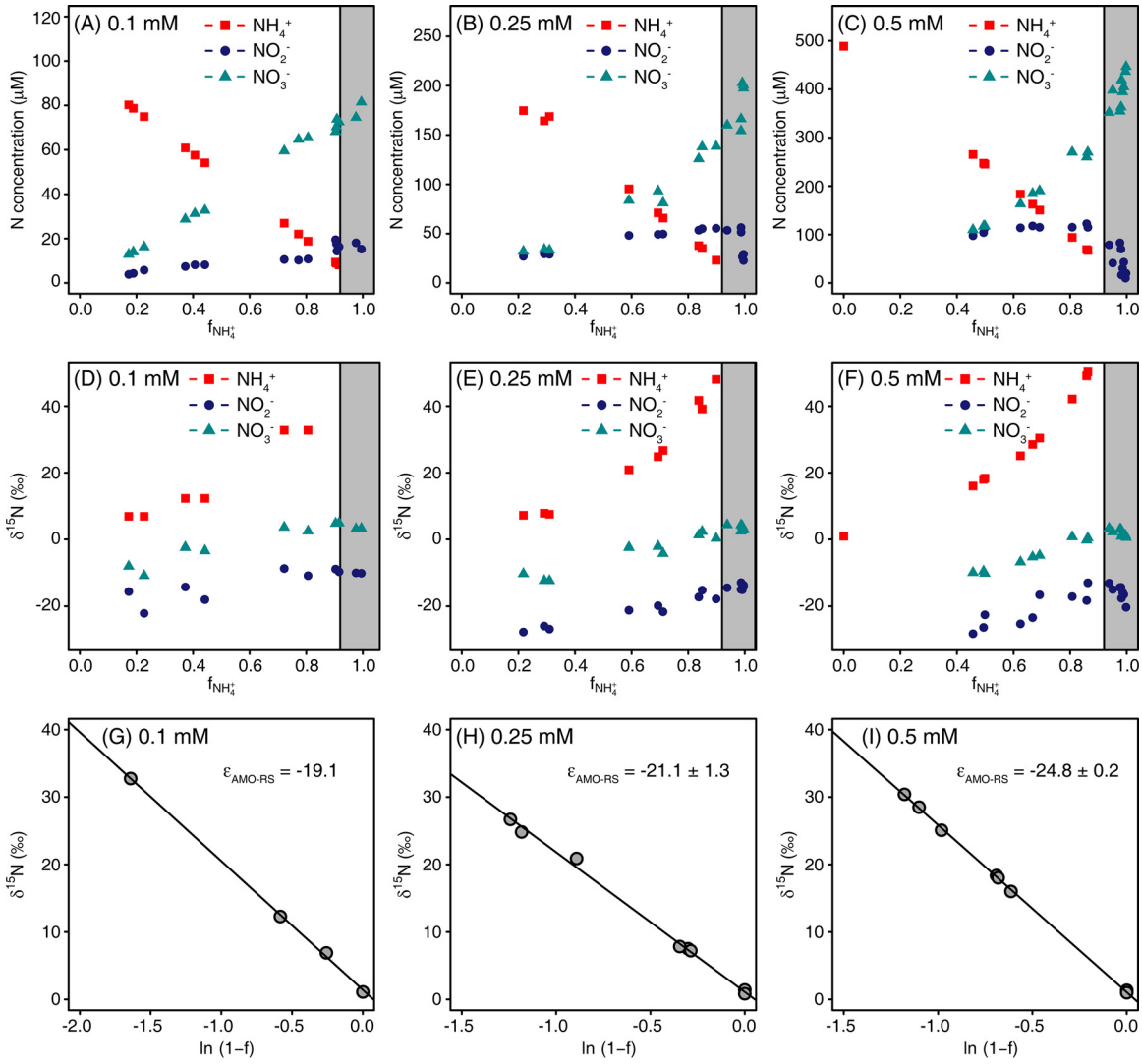

FIG 3 Kinetic isotope effect of *N. inopinata* cultivated in $CaCO_3$-buffered medium with 0.1, 0.25, and 0.5 mM NH_4^+ initial concentration. (A to C) Concentrations of NH_4^+, NO_2^-, and NO_3^-. (D to F) Isotopic signatures of NH_4^+, NO_2^-, and NO_3^-. (G to I) $^{15}\varepsilon_{NH4+\rightarrow NO2-}$ based on the residual substrate ($\varepsilon_{AMO\text{-}RS}$).

Experiment 3: ammonia oxidation with an initial concentration of 0.1, 0.25, and 0.5 mM NH_4^+. Similar patterns of NH_4^+ oxidation, NO_2^- production and consumption, and NO_3^- production were observed for all tested initial NH_4^+ concentrations (Fig. 3A to C). However, the NH_4^+ oxidation rates increased with higher initial NH_4^+ concentrations (Table 1). The concentration of transiently accumulated NO_2^- also increased with the initial NH_4^+ concentration (Fig. 3A to C). The $\delta^{15}N$ of NH_4^+ increased with ongoing NH_4^+ oxidation, along with an increase in the $\delta^{15}N$ of NO_2^- and NO_3^-. After about 93% of the NH_4^+ had been consumed, a pronounced decrease in the $\delta^{15}N$ of NO_2^- was observed, which was consistent with the net consumption of NO_2^- (Fig. 3, especially Fig. 3D to F). The $^{15}\varepsilon_{NH4+\rightarrow NO2-}$ values based on the residual substrate were significantly ($P < 0.05$) larger for the 0.5 mM initial NH_4^+ concentration (−24.8‰) compared to that for the 0.25 mM initial NH_4^+ concentration (−21.1‰). The $^{15}\varepsilon_{NH4+\rightarrow NO2-}$ was smallest (−19.1‰) for the 0.1 mM initial NH_4^+ concentration among all the tested initial NH_4^+ concentrations (Fig. 3G to I). The calculated $^{15}\varepsilon_{NH4+\rightarrow NO2-}$ values based on the cumulative product were similar to those based on the residual substrate, with values of −17.3, −21.2, and −24.3‰ for the 0.1, 0.25, and 0.5 mM NH_4^+ addition, respectively (Table 1). As outlined below (see Discussion), the weaker $^{15}\varepsilon_{NH4+\rightarrow NO2-}$ at the

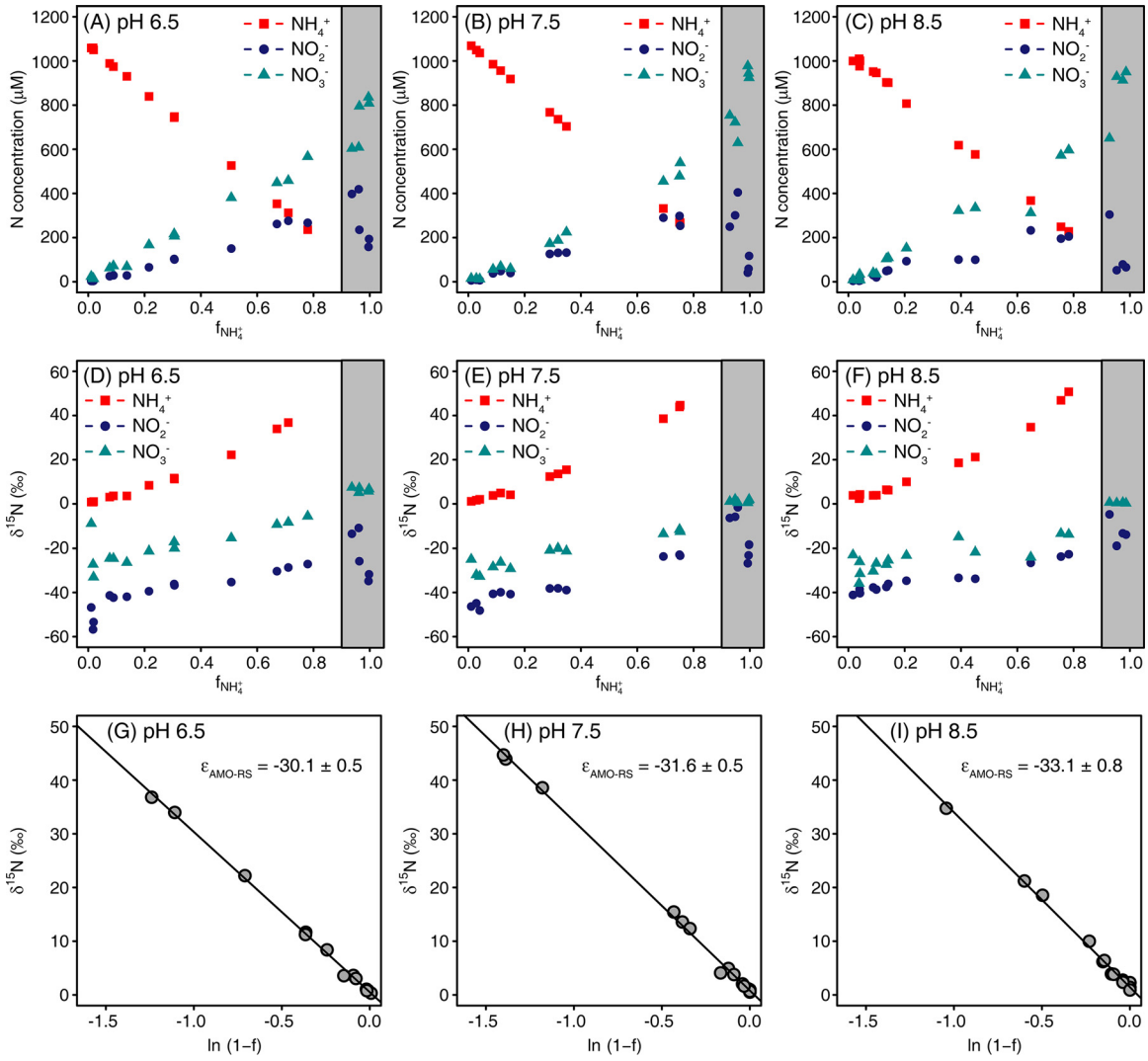

FIG 4 Kinetic isotope effect of *N. inopinata* cultivated with 1 mM NH_4^+ (initial concentration) at pH 6.5, 7.5, and 8.5. (A to C) Concentrations of NH_4^+, NO_2^- and NO_3^-. (D to F) Isotopic signatures of NH_4^+, NO_2^-, and NO_3^-. (G to I) $^{15}\varepsilon_{NH4+\rightarrow NO2-}$ based on the residual substrate ($\varepsilon_{AMO\text{-}RS}$).

lowest NH_4^+ concentration could be due to the low NH_4^+ oxidation rates with 0.1 mM NH_4^+ [2.1 μmol N (mg protein)$^{-1}$ h^{-1}; total protein content was ~2.8 μg ml^{-1}], which was significantly smaller than the V_{max} [12.8 μmol N (mg protein)$^{-1}$ h^{-1}] of *N. inopinata* (21). The $^{15}\varepsilon_{NO2-\rightarrow NO3-}$ values based on the Solver model were 6.2, 10.8, and 10.5‰ for the 0.1, 0.25, and 0.5 mM NH_4^+ treatments, respectively (Table 1). No significant difference of $^{15}\varepsilon_{NO2-\rightarrow NO3-}$ was observed between the 0.25 and 0.5 mM initial NH_4^+ concentration treatments.

Experiment 4: ammonia oxidation at different pH values with an initial concentration of 1 mM NH_4^+. In this experiment, the maximum NH_4^+ oxidation rates (day 3 to 4 for pH 6.5 and 7.5; day 4 to 5 for pH 8.5) were significantly ($P < 0.05$) lower at pH 8.5 than at pH 7.5 (Table 1 and Fig. 4A to C). The NO_2^- concentration was significantly ($P < 0.05$) higher at pH 6.5 (361 μM) than that at pH 8.5 (234 μM), which was consistent with the trend of maximum NO_2^- oxidation rate (this was calculated during the period of NO_2^- oxidation when NH_4^+ was almost completely consumed) that was significantly ($P < 0.05$) lower at pH 6.5 (9.7 μM h^{-1}) than at pH 8.5 (13.5 μM h^{-1}). The δ^{15}N of NH_4^+, NO_2^-, and NO_3^- showed similar patterns as in the other experiments, i.e., the δ^{15}N of NH_4^+, NO_2^-, and NO_3^- increased simultaneously with ammonia oxidation until more than 90% NH_4^+ was oxidized, followed by a decrease in the δ^{15}N of

TABLE 2 Compilation of kinetic isotope effects of canonical AOA, AOB, and NOB

Nitrifier group	Strain	Initial substrate (mM)	pH	ε_{RS} (‰)	ε_{CP} (‰)	Reference
AOA	*Nitrosopumilus adriaticus*	1	7.6	−32 ± 1	−40 ± 1	Mooshammer et al. (33)
	Nitrososphaera viennensis	1−2	7.5	−32 ± 1	−39	Mooshammer et al. (33)
	Nitrososphaera gargensis	0.25	8.2	−22 ± 0	−33 ± 2	This study (Fig. S1 and S2)
	Nitrosocosmicus oleophilus	1	7.5	−36 ± 5	−36 ± 5	This study (Fig. S1 and S2)
	AOA enrichment CN25				−22 ± 5	Santoro and Casciotti (8)
	AOA enrichment CN75	0.01−0.075			−21 ± 10	Santoro and Casciotti (8)
	AOA enrichment CN150				−22 ± 5	Santoro and Casciotti (8)
	"Candidatus *Nitrosocaldus*"	0.2	8.2−8.6		−25 ± 2	Nishizawa et al. (9)
	"Candidatus *Nitrosocaldus*"	14	8.0		−32 ± 1	Nishizawa et al. (9)
AOB	*Nitrosomonas europaea*	4.7−25	7.5	−35 ± 3	−32 ± 6	Mariotti et al. (6)
	Nitrosomonas europaea	38			−32 to −25	Yoshida (30)
	Nitrosomonas europaea	1			−38 ± 2	Casciotti et al. (7)
	Nitrosomonas marina	2			−14 ± 4	Casciotti et al. (7)
	Nitrosomonas sp. C-113a	2	8.0		−19 ± 1	Casciotti et al. (7)
	Nitrosospira tenuis	1			−25 ± 1	Casciotti et al. (7)
	Nitrosomonas eutropha	1			−33 ± 2	Casciotti et al. (7)
	Nitrosomonas sp. C-113a					Casciotti et al. (43)
	Nitrosococcus oceani	0.005−0.05	8.2		−46 to −30	Casciotti et al. (43)
	Nitrosospira briensis					Casciotti et al. (43)
NOB	*Nitrococcus mobilis*			20 ± 3		Buchwald and Casciotti (11)
	Nitrobacter sp. Nb 355	0.05	8.2	21 ± 3		Buchwald and Casciotti (11)
	Nitrospira marina			9 ± 2		Buchwald and Casciotti (11)
	Nitrospira sp. Ecomares 2.1	0.5−1	7.5	10 ± 1		Jacob et al. (14)
	Nitrospina watsonii 347	0.6−1.6		10 ± 1		Jacob et al. (14)
	Nitrospira moscoviensis	1	7.5	9 ± 1		This study (Fig. S3)

NO_2^- until the end of the incubations (Fig. 4D to F). There was no significant difference for the $^{15}\varepsilon_{NH4^+\rightarrow NO2^-}$ calculated based on the residual substrate among the three pH levels (Table 1 and Fig. 4G to I), but the $^{15}\varepsilon_{NH4^+\rightarrow NO2^-}$ based on product formation was significantly ($P < 0.05$) weaker at pH 6.5 than at pH 7.5 and pH 8.5 (Table 1). Interestingly, the $\delta^{15}N$ of NO_2^- was significantly ($P < 0.05$) lower at pH 6.5 than at pH 8.5 at the beginning of the experiment. Moreover, the pH affected the isotope effect of NO_2^- oxidation significantly, where the $^{15}\varepsilon_{NO2^-\rightarrow NO3^-}$ was significantly ($P < 0.05$) weaker at pH 8.5 than that at pH 7.5 and 6.5, based on the Solver model (Table 1).

DISCUSSION

Isotope effects of ammonia and nitrite oxidation by *N. inopinata*. The measured N isotope effect for ammonia oxidation ($^{15}\varepsilon_{NH4^+\rightarrow NO2^-}$) by *N. inopinata* (residual substrate [RS], −33.0 to −30.7‰; cumulative product [CP], −35.5 to −31.2‰) with an initial substrate concentration of 1 mM NH_4^+ fell into the range of $^{15}\varepsilon_{NH4^+\rightarrow NO2^-}$ values determined previously for AOB (−38.2 to −14.2‰) and AOA (−41 to −13‰) (7–9) (Table 2), as well as the measured N isotope effect of the two AOA species *Nitrososphaera gargensis* (RS, −22.3‰; CP, −32.8‰) and *Nitrosocosmicus oleophilus* that were also determined in this study (RS, −36.1‰; CP, −36.3‰) (see Fig. S1 and S2 in the supplemental material). However, isotope fractionation data are currently still lacking for many phylogenetic lineages of AOB and AOA. The most similar isotope effects, compared with *N. inopinata*, have been reported for *Nitrosomonas europaea*

(−38.2‰) and *Nitrosomonas eutropha* (−32.8‰) (6, 7) (Table 2). In this context, it is noteworthy that comammox *Nitrospira*, betaproteobacterial AOB, and AOA possess three phylogenetically different types of AMO (16, 17, 23). Moreover, the characterized comammox *Nitrospira* and many AOA have a much higher substrate affinity for NH_3 than AOB (21, 24, 25). Despite the distinct phylogenetic and kinetic properties of the AMO forms, no difference in the magnitude of $^{15}\varepsilon_{NH4+\rightarrow NO2-}$ between comammox, AOB, and AOA became apparent. This result may indicate that the enzymatic mechanism and transition states of the NH_3 oxidation step catalyzed by AMO are similar across all ammonia oxidizers. However, the reported $^{15}\varepsilon_{NH4+\rightarrow NO2-}$ values varied strongly, even within one species or strain, in previous research (7–9). Hence, the kinetic isotope effects of ammonia oxidizers may be modulated by environmental factors, some of which have been investigated in our study (see below).

Like canonical NOB (10, 11, 14), *N. inopinata* displayed an inverse $^{15}\varepsilon_{NO2\rightarrow NO3-}$, meaning that $^{15}NO_2^-$ was preferentially oxidized to NO_3^- during NO_2^- oxidation. The measured value of $^{15}\varepsilon_{NO2\rightarrow NO3-}$ (9.2‰ ± 0.5‰ at pH 8.2 and 1 mM NO_2^-) was in line with previously determined $^{15}\varepsilon_{NO2\rightarrow NO3-}$ values (9.1 to 10.2‰) of canonical *Nitrospira* NOB (11, 14) (Table 2 and Fig. S3). The NXR of *N. inopinata* clusters together with the NXR of canonical *Nitrospira* in phylogenetic analyses of the substrate-binding alpha subunit and the electron-channeling beta subunit of this enzyme (16). This close phylogenetic relationship is consistent with the highly similar kinetic isotope effects of comammox and canonical *Nitrospira*. Other NOB such as *Nitrobacter* (20.6‰) and *Nitrococcus* (12.8‰) showed remarkably stronger kinetic isotope effects than *Nitrospira* (10, 11). Interestingly, *Nitrobacter* and *Nitrococcus* have a lower whole-cell affinity (higher $K_{m(app)}$) for NO_2^- than *Nitrospira* (14, 22). Therefore, the differences in the kinetic isotope effect were suggested to be linked to the NO_2^- affinity of NOB, possibly caused by a different stability of the transition state in high- versus low-affinity NXR forms (14). However, this explanation turns out to be unlikely, considering that the isotope effect of the NXR of *N. inopinata* resembles that of other *Nitrospira* strains, whereas its whole-cell nitrite affinity is low and in the same range as the whole-cell affinity of *Nitrobacter* species (21). Instead, it may be more relevant that the NXR of *Nitrospira* (including comammox species) is located in the periplasmic space (where it may interact with the cytoplasmic membrane), whereas the membrane-attached NXR of *Nitrobacter* and *Nitrococcus* is oriented toward the cytoplasm (references 26 and 27 and references cited therein). The cellular localization of NXR determines whether transport of NO_2^- and NO_3^- over the cytoplasmic membrane is needed, which might also influence the kinetic isotope effect through the properties of the nitrite/nitrate transporter: it may limit the expression of the isotope effect of NXR if NO_2^- transport (has almost no isotope fractionation as a diffusional process) becomes limiting relative to NXR activity. The localization of NXR also affects the energy efficiency of nitrite oxidation, because only a periplasmic NXR contributes directly to proton motive force (26, 28). Moreover, the periplasmic and cytoplasmic NXR types represent phylogenetically unrelated lineages within the type II dimethyl sulfoxide (DMSO) reductase-like family of molybdopterin-containing enzymes (26, 29). The different magnitude of the kinetic isotope effect in NOB likely reflects the distinct functional properties and evolutionary history of the periplasmic and cytoplasmic NXR forms. This possibility was discussed previously (14) and gains further support from our results.

Effects of substrate concentration and pH on the kinetic isotope effects of comammox bacteria. Nitrogen isotope effects of ammonia oxidizers varied largely among previous studies, even within AOB and AOA (7–9). This variability might partly be caused by different enzyme (AMO) structures. However, a substantial variation in kinetic isotope effects can occur even within a single isolate, as reported for the AOB species *Nitrosomonas europaea* (6, 7, 30). Such variability indicates that the cultivation conditions and growth stage and specific factors, such as concentration-dependent diffusion limitations of substrate availability for the critical enzyme or the accumulation of intermediates in an N transformation pathway, can significantly affect the kinetic isotope effect (illustrated in Fig. 5). For comammox, possible effects of environmental conditions on the kinetic isotope effects of ammonia oxidation and nitrite oxidation,

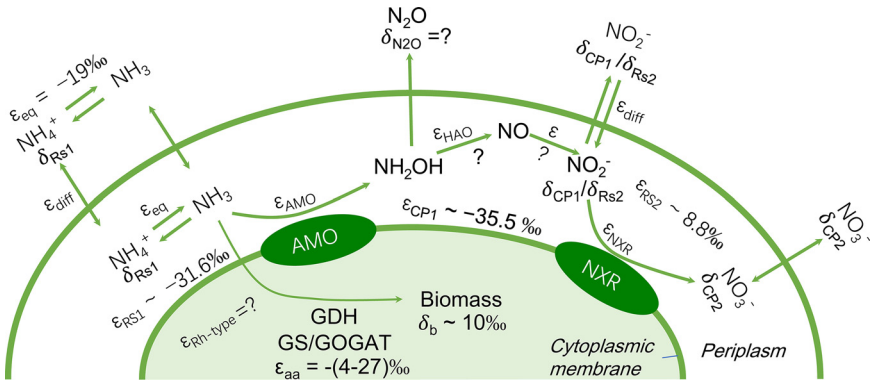

FIG 5 Schematic overview of N processes and isotope fractionation effects involved in NH_3 oxidation, NO_2^- oxidation, formation of intermediates, and growth of the comammox strain *Nitrospira inopinata*. Average kinetic isotope effects of NH_3 and NO_2^- oxidation are presented for the residual substrate (NH_4^+, ε_{RS1}; NO_2^-, ε_{RS2}) and the cumulative product (NO_2^-, ε_{CP1}) with the addition of 1 mM NH_4^+ at pH 7.5. Isotope fractionation of NH_3/NH_4^+ equilibration and NH_3 uptake refer to reference 32. This schematic illustration is modified from reference 33.

respectively, have not yet been studied. Here, we analyzed the effects of two conditions, the initial NH_4^+ concentration and culture pH, on the kinetic isotope effects of complete nitrification by *N. inopinata*.

Previous studies with AOB and AOA mostly found $^{15}\varepsilon$ to be below −20‰, which is the range seen in our experiments with comammox at high initial NH_4^+ concentrations (Tables 1 and 2). However, we observed salient decreasing trends of $^{15}\varepsilon_{NH4+\rightarrow NO2-}$ with decreasing NH_4^+ concentrations between 1 and 0.1 mM. This result is consistent with previous data from an enrichment of thermophilic canonical AOA, where smaller isotope effects were found at lower NH_4^+ concentrations (0.25 mM) compared to those in experiments with high NH_4^+ concentrations (10 mM) (9). Also for denitrifiers, a decrease of the N isotope effect was observed along with decreasing NO_3^- concentrations in the medium (31). In our study, the NH_3 oxidation rates were lower at 0.1 mM NH_4^+ [2.1 μmol N (mg protein)$^{-1}$ h^{-1}] than at 0.25 mM [3.1 μmol N (mg protein)$^{-1}$ h^{-1}] and 0.5 mM NH_4^+ [3.8 μmol N (mg protein)$^{-1}$ h^{-1}], which were much lower than the V_{max} [12.8 μmol N (mg protein)$^{-1}$ h^{-1}] of *N. inopinata* (21). Thus, the rate-limiting step for NH_3 oxidation at low NH_4^+ concentrations was probably more dependent on NH_3 diffusion/transport from the extracellular space into the periplasm, where the active sites of the enzymes involved in ammonia oxidation are likely located. Therefore, under these conditions, $^{15}\varepsilon_{NH4+\rightarrow NO2-}$ did not reflect the enzymatic isotope effect, but rather the equilibrium isotope effect $^{15}\varepsilon_{NH4+\rightarrow NH3}$ at low NH_4^+ concentrations, which is around −19‰ (32). However, when NH_4^+ concentrations are higher and transport does not limit the AMO activity, enzymatically catalyzed NH_3 oxidation will become the limiting step, and $^{15}\varepsilon_{NH4+\rightarrow NO2-}$ based on the residual substrate (ε_{RS1}) will converge to the enzymatic isotope effect of AMO. Moreover, the isotope effect based on ε_{RS1} is also influenced by NH_4^+ assimilation for biomass formation and can therefore diverge from that based on residual substrate of ammonia oxidation. Compared to ε_{RS1}, $^{15}\varepsilon_{NH4+\rightarrow NO2-}$ based on product formation (ε_{CP1}) is affected by other factors, including N intermediate (NH_2OH and NO) accumulation and N gas (N_2O and NO) loss. Mooshammer et al. (33) demonstrated N assimilation to be the main factor responsible for the difference between ε_{RS1} and ε_{CP1} in the AOA species *Nitrososphaera viennensis*. In our experiment, we did not observe any significant change in the total protein content of the *N. inopinata* cultures at 0.1, 0.25, and 0.5 mM NH_4^+ during the incubation. The absence of detectable growth may explain the similar isotope effects of ε_{RS1} and ε_{CP1} at all three NH_4^+ concentrations. It appears that the NH_4^+ concentration also influenced the isotope effect of NO_2^- oxidation, as the modeled $^{15}\varepsilon_{NO2-\rightarrow NO3-}$ was considerably smaller at the lowest tested initial NH_4^+ concentration (0.1 mM; Table 1). The

reason could be the low maximal NO_2^- concentration (around 10 μM) during NH_3 and NO_2^- oxidation with 0.1 mM NH_4^+ (Fig. 3A). *N. inopinata* has quite a poor affinity (372 $\pm$ 55 μM) for NO_2^- during NO_2^- oxidation (21), and NO_2^- accumulated to higher concentrations in the experiments with 0.25 and 0.5 mM NH_4^+ (Fig. 3B and C). Accordingly, the kinetic isotope effect of NO_2^- oxidation was more pronounced at these higher concentrations (Table 1).

Medium pH is another factor potentially affecting kinetic isotope effects. *N. inopinata* has strong activities of NH_3 and NO_2^- oxidation in the pH range of 6.5 to 8.5, with lower NH_3 oxidation rates at pH 8.5 than those at pH 7.5 (Table 1). The NH_3 oxidation rates were not significantly different between pH 6.5 and 7.5, while the NO_2^- oxidation rates (which were calculated in the later period of NH_3 oxidation when NH_4^+ was almost completely consumed) were significantly lower at pH 6.5 than that at pH 8.5. The pH also influenced the $^{15}\varepsilon_{NH4+\rightarrow NO2-}$ and $^{15}\varepsilon_{NO2-\rightarrow NO3-}$. The ε_{RS1} did not change significantly among different pH values, while the ε_{CP1} was much lower at pH 6.5 than that at pH 7.5 and pH 8.5 (Table 1). As discussed before, ε_{CP1} was probably affected by the isotopic fractionation during intermediate formation (33). With *N. inopinata* cultures, release of small amounts of NH_2OH, NO, and N_2O from cells has been observed during the oxidation of NH_3 to NO_2^- (34, 35). Any pH-dependent shifts in the amounts of these released compounds could lead to changes of $^{15}\varepsilon_{NH4+\rightarrow NO2-}$ (Fig. 5).

A pH-dependent shift was also observed for the $^{15}\varepsilon_{NO2-\rightarrow NO3-}$, which decreased significantly from 11.1‰ to 6.0‰ when the pH increased from 6.5 to 8.5 (Table 1). As stated above, we assume that a limited NO_2^- availability caused the observed decrease of $^{15}\varepsilon_{NO2-\rightarrow NO3-}$ in the experiment with an initial NH_4^+ concentration of only 0.1 mM (Table 1). We observed that the concentration of transiently accumulated NO_2^- was lowest at pH 8.5 (compared to pH 6.5 and 7.5) during the whole NH_3 oxidation period (Fig. 4A to C), which was in agreement with the lower rate of NH_3 oxidation at pH 8.5 (Table 1). In addition, the maximum NO_2^- oxidation rate was higher at pH 8.5 than that at pH 6.5 and 7.5. Thus, the relatively high rate of NO_2^- oxidation and low rate of NH_3 oxidation together led to the lower NO_2^- concentrations and thus can make NO_2^- diffusion the limiting step for NO_2^- oxidation at pH 8.5, especially for *N. inopinata* that has a low affinity for NO_2^- during NO_2^- oxidation. The effect of pH on NO_2^- self-decomposition was unlikely the cause of the different isotope effect in the pH range of 6.5 to 8.5. In our experiments, we found no significant change of the N balance and of $\delta^{15}N_{NH3+NO2+NO3}$ at pH 6.5 to 8.5 (Fig. S4). This is consistent with the findings of Casciotti et al. (10), where no change of $\delta^{15}N$ was observed in the $\delta^{15}N_{NO2+NO3}$ in incubations of nitrite oxidizers and in control flasks in the pH range of 7.8 to 8.8. Until now, there has been no systematic investigation of the pH effect on $^{15}\varepsilon_{NO2-\rightarrow NO3-}$ of canonical NOB. Recently, a new NOB from the genus *Nitrospira* has been cultivated from an alkaline lake (36). It would be worthy to explore the $^{15}\varepsilon_{NO2-\rightarrow NO3-}$ of alkali-tolerant NOB and the mechanisms of NO_2^- oxidation at alkaline conditions in further studies.

Conclusions. In summary, our results demonstrate that the $^{15}\varepsilon_{NH4+\rightarrow NO2-}$ and $^{15}\varepsilon_{NO2-\rightarrow NO3-}$ of comammox *N. inopinata* ranged from −33‰ to −27‰ and 6.5‰ to 9‰, respectively, with nonlimiting NH_4^+ and NO_2^- supply as the substrates at pH 7.5 to 8.5. Both substrate concentration and pH affected the $^{15}\varepsilon_{NH4+\rightarrow NO2-}$ and $^{15}\varepsilon_{NO2-\rightarrow NO3-}$ of *N. inopinata* during NH_3 oxidation. At low NH_4^+ concentrations, especially when NH_3 oxidation rates were much smaller than the V_{max} of *N. inopinata*, the $^{15}\varepsilon_{NH4+\rightarrow NO2-}$ was closer to $^{15}\varepsilon_{NH4+\rightarrow NH3}$ and did not reflect the enzymatic isotope effect of *N. inopinata*. Medium pH affected the $^{15}\varepsilon_{NH4+\rightarrow NO2-}$ of *N. inopinata* based on the cumulative product, due to the effect of pH on intermediate formation of *N. inopinata*. The exact reasons responsible for the weaker isotope effects of $^{15}\varepsilon_{NO2-\rightarrow NO3-}$ at higher pH remained elusive. Further studies should target the effects of pH and substrate concentration on the kinetic isotope effects of canonical AOB, AOA, and NOB to investigate the underlying mechanisms.

MATERIALS AND METHODS

Cultivation of *Nitrospira inopinata*. Cultures of *N. inopinata* were maintained at 37°C with 1 mM NH_4Cl in a $CaCO_3$-buffered AOM medium containing (per liter) (37): 50 mg KH_2PO4, 50 mg $MgSO_4 \cdot 7H_2O$,

75 mg KCl, 584 mg NaCl, 4 g $CaCO_3$ (solid buffer), 1 ml selenium-tungstate solution (SWS), and 1 ml trace element solution (TES). For the composition of TES and SWS, please refer to Widdel et al. (38). The pH of the medium was maintained at approximately 8.2. The cultivation conditions and experiments for *Nitrososphaera gargensis*, *Nitrosocosmicus oleophilus*, and *Nitrospira moscoviensis* are described in Text S1 in the supplemental material.

Incubation experiments. (i) Experiment 1: ammonia oxidation with an initial concentration of 1 mM NH_4^+. Metabolically active (i.e., ammonia-oxidizing) *N. inopinata* cells (190 ml) were harvested by centrifugation (5,000 × *g*, 30 min), washed twice with $CaCO_3$-buffered medium (pH ~8.2), and resuspended in 300 ml of $CaCO_3$-buffered medium containing 1 mM NH_4^+. Subsequently, the cell suspension was equally distributed into three autoclaved 250-ml glass bottles. On days 0, 7, 9, 13, and 14 after inoculation, 8-ml aliquots of each replicate were transferred into 15-ml plastic tubes and centrifuged (10,000 × *g*, 10 min). Aliquots (1 ml) of the supernatant were transferred into 1-ml Eppendorf tubes for NO_2^- and NO_3^- isotope analysis, respectively, and 5-ml aliquots of the supernatant were transferred into 15-ml plastic tubes for NH_4^+ isotope analysis. All aliquots of supernatants were frozen at −20°C immediately after sampling.

(ii) Experiment 2: nitrite oxidation with an initial concentration of 1 mM NO_2^-. Metabolically active *N. inopinata* cells (2,000 ml) were harvested by centrifugation (5,000 × *g*, 30 min), washed once, and resuspended in 120 ml of $CaCO_3$-buffered medium containing 1 mM NO_2^-. The cell suspension was equally distributed into three autoclaved 100-ml glass bottles. Samples were taken at 0, 11, 23, 35, and 47 h after inoculation and were centrifuged and stored as described above for experiment 1.

(iii) Experiment 3: ammonia oxidation with an initial concentration of 0.1, 0.25, and 0.5 mM NH_4^+. Metabolically active *N. inopinata* cells (700 ml) were harvested by centrifugation (5,000 × *g*, 30 min), washed once, and resuspended in 1,000 ml of $CaCO_3$-buffered medium without NH_4^+. Subsequently, 900 ml of the cell suspension was equally split into nine autoclaved 250-ml glass bottles. For the different NH_4^+ treatments, 0.02, 0.05, and 0.1 ml of a sterile 0.5 M NH_4^+ solution was added to three bottles, respectively, resulting in triplicates per NH_4^+ concentration. Samples were taken at 0, 4, 7.5, 16.5, 22, and 28 h (0.1 mM NH_4^+), at 0, 7.5, 16.5, 22, 28, and 46 h (0.25 mM NH_4^+), and at 0, 22, 31.5, 43, 54, and 66 h (0.5 mM NH_4^+) after inoculation. The samples were centrifuged and stored as described above for experiment 1.

(iv) Experiment 4: ammonia oxidation at different pH values with an initial concentration of 1 mM NH_4^+. A stock culture of *N. inopinata* was transferred from $CaCO_3$-buffered medium to medium buffered with 2 mM $NaHCO_3$, followed by two rounds of growth and transfer in this medium, in order to remove solid $CaCO_3$. Metabolically active cells (1,200 ml) were then harvested by centrifugation (8,000 × *g*, 15 min), washed with 2 mM $NaHCO_3$-buffered medium, and resuspended in 10 ml of the same medium. This cell suspension was used to inoculate nine glass bottles containing 100 ml medium. During the incubations, 10 mM MES [2-(*N*-morpholino)ethanesulfonic acid], 10 mM HEPES (4-(2-hydroxyethyl)-1-piperazineethanesulfonic acid), and 10 mM TAPS ([tris(hydroxymethyl)methylamino] propanesulfonic acid) were used as buffers to adjust the pH to 6.5, 7.5, and 8.5, respectively. The MES stock buffer was prepared by dissolving 9.76 g MES in 100 ml of 136 mM NaOH. The HEPES stock buffer was prepared by dissolving 23.83 g HEPES in 100 ml of 600 mM NaOH. The TAPS stock buffer was prepared by dissolving 24.3 g TAPS in 100 ml of 570 mM NaOH. Buffer stock solutions were diluted to 10 mM MES, HEPES, and TAPS, respectively, and sterilized. 1 M HCl and 1 M NaOH were used to adjust the pH to 6.5, 7.5, and 8.5. For each pH treatment, samples were taken on 0, 0.3, 1.3, 2.3, 3.3, 4.3, 5.3, 6.5, and 8.5 days after inoculation. The samples were centrifuged and stored as described above for experiment 1.

Chemical analyses. Inorganic N concentrations were measured by using established protocols (39). Combined NH_3 and NH_4^+ concentrations were determined by the indophenol blue method. NO_2^- concentrations were measured spectrophotometrically by the Griess reaction after reaction with sulfanilamide and *N*-1-naphthyl-ethylenediamine dihydrochloride. NO_3^- concentrations were measured by the Griess reaction after reduction to NO_2^- with vanadium chloride. Total protein concentrations were measured by the Bradford assay.

Nitrogen isotope analyses. The $\delta^{15}N$ values of NH_4^+ were analyzed by microdiffusion coupled to elemental analyzer-isotope ratio mass spectrometry (EA-IRMS [40]). For isotopic calibration, the following NH_4^+ standards were used: IAEA-N-2 (20.3‰ ± 0.2‰), IAEA-N-1 (0.4‰ ± 0.2‰), and USGS26 (53‰ ± 0.4‰). The $\delta^{15}N$ signatures of NO_2^- and NO_3^- were measured by purge-and-trap isotope ratio mass spectrometry (PT-IRMS) after chemical conversion of NO_2^- and NO_3^- to N_2O (40). In-house NO_2^- and NO_3^- standards, which ranged between −20.5 and 16.8‰, were used for isotopic calibration and were analyzed in parallel with the samples.

Natural ^{15}N abundances are defined in the delta notation as follows: $\delta^{15}N$ (‰) = $[(^{15}N_{sample}/^{14}N_{sample})/(^{15}N_{std}/^{14}N_{std}) - 1] \times 1{,}000$ where std stands for standard. Isotope ratios are reported relative to AIR (atmospheric dinitrogen).

Kinetic isotope effects were defined as follows:

$$\varepsilon_k = \left(\frac{k_H}{k_L} - 1\right) \times 1000 \quad (1)$$

where k_L is the first-order rate constant for the reaction of isotopically light molecules (e.g., ^{14}N) and k_H is the rate constant for the reaction of isotopically heavy molecules (e.g., ^{15}N). The organism-level nitrogen isotope effect for ammonia oxidation ($^{15}\varepsilon_k$ $\sum NH_3/NO_2^-$) was calculated using the

Rayleigh residual substrate (RS) equation (equation 2) and the cumulative product (CP) equation (equation 3):

$$\delta_{RS} = \delta_{\text{input}} + \varepsilon_k \times \ln(1-f) \tag{2}$$

$$\delta_{\text{CP}} = \delta_{\text{input}} - \varepsilon_k \ln(1-f)\frac{(1-f)}{f} \tag{3}$$

where δ_{RS} is the N isotope signature of the residual substrate, i.e., NH_3 (in the case of NH_3 oxidation) or of NO_2^- (in the case of NO_2^- oxidation); δ_{CP} is the N isotope signature of the cumulative product, i.e., NO_2^- (in the case of NH_3 oxidation) or NO_3^- (in the case of NO_2^- oxidation); δ_{input} is the substrate isotope signal initially present in the medium, and f is the oxidizing fraction of substrate. $\delta^{15}N$ at any time since the initial time point was calculated from the measured $\delta^{15}N$ using the following isotope mass balance equation:

$$\delta^{15}\text{N} = \frac{(\delta^{15}\text{N}_{\text{con.}}[\text{N}_{\text{con.}}] - \delta^{15}\text{N}_{\text{initial}}[\text{N}_{\text{initial}}])}{([\text{N}_{\text{con.}}] - [\text{N}_{\text{initial}}])} \tag{4}$$

where $N_{\text{con.}}$ is the measured concentration of a specific substrate or product, which includes the background from initial cultures plus the added substrates, and N_{initial} is the concentration of substrates transferred with the initial cultures, i.e., the background concentrations of substrates. Initial measurements of the $\delta^{15}N$ signatures of NH_4^+, NO_2^-, and NO_3^-, deriving from transferring the cultures to new media, when starting new experiments, were done for time zero, and corrected for from the following culture samples using mass and isotope balance equations (41).

Solver model. An isotope fractionation model was constructed based on linearly connected, closed system isotope fractionation submodels depicting the coupled sequential processes of nitrification. We assumed that the processes in all incubations were operating under closed system conditions as shown elsewhere (6). Three processes were considered and incorporated in the model in sequential order: (i) NH_3 oxidation (AO), (ii) NO_2^- production (NiP), and (iii) NO_2^- oxidation to NO_3^- (NiO). AO can also include isotope effects of equilibrium isotope fractionation between NH_3 and NH_4^+ and of NH_4^+ uptake and is distinguished from NiP, because the kinetic isotope effect of RS and CP of NH_3 oxidation can differ (33). The reason is that multiple processes consume NH_3/NH_4^+, which is used for biomass formation and NH_3 oxidation, and that the NH_3 oxidation pathway in nitrifiers comprises several intermediates and byproducts (hydroxylamine, nitric oxide, and nitrous oxide), which can also change the isotope effect as determined by RS and CP. The model is therefore composed of a system of nine equations (equations 5 to 13). It uses the measured N compound concentrations ($NH_4^+{}_{\text{initial}}$, $NH_4^+{}_{\text{residual}}$, $NO_2^-{}_{\text{residual}}$, and $NO_3^-{}_{\text{cumulative}}$) and their $\delta^{15}N$ values ($\delta^{15}N_{\text{NH4+ initial}}$, $\delta^{15}N_{\text{NH4+ residual}}$, $\delta^{15}N_{\text{NO2- residual}}$, and $\delta^{15}N_{\text{NO3- cumulative}}$) to simulate the kinetic isotopic effects (ε) and fractions (f, $0 \leq f \leq 1$) of N sources converted to N sinks in the three listed processes. Therefore, for the three coupled processes, we derive:

$$\delta^{15}\text{N}_{\text{NH4 + residual}} = \delta^{15}\text{N}_{\text{NH4 + initial}} + \varepsilon_{\text{AO}} \times \ln(1 - f_{\text{AO}}) \tag{5}$$

$$\delta^{15}\text{N}_{\text{NO2}-\text{ cumulative}} = \delta^{15}\text{N}_{\text{NH4 + initial}} - \varepsilon_{\text{NiP}}(1 - f_{\text{AO}})\frac{\ln(1 - f_{\text{AO}})}{f_{\text{AO}}} \tag{6}$$

$$\text{NH}_4^+{}_{\text{ residual}} = \text{NH}_4^+{}_{\text{ initial}}(1 - f_{AO}) \tag{7}$$

$$\text{NO}_2^-{}_{\text{ cumulative}} = \text{NH}_4^+{}_{\text{ initial}} f_{\text{NiP}} \tag{8}$$

$$\delta^{15}\text{N}_{\text{NO2}-\text{ initial}} = \delta^{15}\text{N}_{\text{NO2}-\quad\text{product}} \tag{9}$$

$$\delta^{15}\text{N}_{\text{NO2}-\text{residual}} = \delta^{15}\text{N}_{\text{NO2}-\text{initial}} + \varepsilon_{\text{NiO}}\ln(1 - f_{\text{NiO}}) \tag{10}$$

$$\delta^{15}\text{N}_{\text{NO3}-\text{ cumulative}} = \delta^{15}\text{N}_{\text{NO2}-\text{initial}} - \varepsilon_{\text{NiO}}(1 - f_{NiO})\frac{\ln(1 - f_{\text{NiO}})}{f_{\text{NiO}}} \tag{11}$$

$$\text{NO}_2^-{}_{\text{ residual}} = \text{NO}_2^-{}_{\text{ initial}}(1 - f_{\text{NiO}}) \tag{12}$$

$$\text{NO}_3^-{}_{\text{ cumulative}} = \text{NO}_2^-{}_{\text{ initial}} f_{\text{NiO}} \tag{13}$$

where ε_{AO}, ε_{NiP}, and ε_{NiO} represent the kinetic isotopic effects of NH_3 oxidation, NO_2^- production, and NO_2^- oxidation, respectively. The corresponding N fractions are denoted as f_{AO}, f_{NiP}, and f_{NiO}. This system of equations was set up in Microsoft Excel and solved by the SOLVER macro in Microsoft Office Excel. The following setting was used: set objective ($\delta^{15}N_{\text{TDN}}$ as measured). The variable cells (all ε and f values of all processes) are solved so that all modeled RS and CP values (concentrations and $\delta^{15}N$ signatures)

conform to the measured values. The ranges of variable cells (ε and f values) for each process were subject to constraints (see Table S1 in the supplemental material) with reference to published synthesis studies (7–10, 14, 33). The model was run for each incubation experiment and replicate individually, based on 1,000 iterations and using the GRG nonlinear engine as the solving method. Model accuracy across all incubation experiments was examined by regressing the simulated N contents and δ^{15}N values of individual N pools against the corresponding measured values. Model results with an adjusted R^2 of >0.95 were accepted. Otherwise, variable constraints were adapted and outliers were deleted eventually.

Statistical analyses. Analysis of variance (ANOVA) was used to test the effects of pH and concentration levels on the isotope effects of $^{15}\varepsilon_{NH4+\rightarrow NO2-}$ and $^{15}\varepsilon_{NO2-\rightarrow NO3-}$ using the R software package (version 3.4.3 [42]). Tukey's tests ($P < 0.05$) were used to examine significant differences between the means of kinetic isotope effects at different pH or concentration levels.

SUPPLEMENTAL MATERIAL

Supplemental material is available online only.

TEXT S1, PDF file, 0.1 MB.

FIG S1, TIF file, 0.1 MB.

FIG S2, TIF file, 0.1 MB.

FIG S3, TIF file, 0.03 MB.

FIG S4, TIF file, 0.04 MB.

TABLE S1, PDF file, 0.1 MB.

ACKNOWLEDGMENTS

This research was supported by the Comammox Research Platform funded by the University of Vienna and by Austrian Science Fund (FWF) project P30570-B29 to H.D.

We are grateful to Margarete Watzka for help with EA-IRMS analyses, Ludwig Seidl and Sabrina Pober for ordering experimental materials, Christopher Sedlacek for providing the comammox pure culture, and Petra Pjevac for helpful discussions.

REFERENCES

1. Houlton BZ, Sigman DM, Hedin LO. 2006. Isotopic evidence for large gaseous nitrogen losses from tropical rainforests. Proc Natl Acad Sci U S A 103:8745–8750. https://doi.org/10.1073/pnas.0510185103.
2. Casciotti KL. 2016. Nitrite isotopes as tracers of marine N cycle processes. Philos Trans R Soc A 374:20150295. https://doi.org/10.1098/rsta.2015.0295.
3. Denk TRA, Mohn J, Decock C, Lewicka-Szczebak D, Harris E, Butterbach-Bahl K, Kiese R, Wolf B. 2017. The nitrogen cycle: a review of isotope effects and isotope modeling approaches. Soil Biol Biochem 105:121–137. https://doi.org/10.1016/j.soilbio.2016.11.015.
4. Bai E, Houlton BZ. 2009. Coupled isotopic and process-based modeling of gaseous nitrogen losses from tropical rain forests. Global Biogeochem Cycles 23:1–10.
5. van Dam D, van Breemen N. 1995. NICCE: a model for cycling of nitrogen and carbon isotopes in coniferous forest ecosystems. Ecol Model 79:255–275. https://doi.org/10.1016/0304-3800(94)00184-J.
6. Mariotti A, Germon JC, Hubert P, Kaiser P, Letolle R, Tardieux A, Tardieux P. 1981. Experimental determination of nitrogen kinetic isotope fractionation: some principles; illustration for the denitrification and nitrification processes. Plant Soil 62:413–430. https://doi.org/10.1007/BF02374138.
7. Casciotti KL, Sigman DM, Ward BB. 2003. Linking diversity and stable isotope fractionation in ammonia-oxidizing bacteria. Geomicrobiol J 20:335–353. https://doi.org/10.1080/01490450303895.
8. Santoro AE, Casciotti KL. 2011. Enrichment and characterization of ammonia-oxidizing archaea from the open ocean: phylogeny, physiology and stable isotope fractionation. ISME J 5:1796–1808. https://doi.org/10.1038/ismej.2011.58.
9. Nishizawa M, Sakai S, Konno U, Nakahara N, Takaki Y, Saito Y, Imachi H, Tasumi E, Makabe A, Koba K, Takai K. 2016. Nitrogen and oxygen isotope effects of ammonia oxidation by thermophilic Thaumarchaeota from a geothermal water stream. Appl Environ Microbiol 82:4492–4504. https://doi.org/10.1128/AEM.00250-16.
10. Casciotti KL. 2009. Inverse kinetic isotope fractionation during bacterial nitrite oxidation. Geochim Cosmochim Acta 73:2061–2076. https://doi.org/10.1016/j.gca.2008.12.022.
11. Buchwald C, Casciotti KL. 2010. Oxygen isotopic fractionation and exchange during bacterial nitrite oxidation. Limnol Oceanogr 55:1064–1074. https://doi.org/10.4319/lo.2010.55.3.1064.
12. Casciotti KL, McIlvin MR. 2007. Isotopic analyses of nitrate and nitrite from reference mixtures and application to Eastern Tropical North Pacific waters. Mar Chem 107:184–201. https://doi.org/10.1016/j.marchem.2007.06.021.
13. Westaway KC. 2006. Using kinetic isotope effects to determine the structure of the transition states of SN2 reactions. Adv Phys Org Chem 41:217–273.
14. Jacob J, Nowka B, Merten V, Sanders T, Spieck E, Dähnke K. 2017. Oxidation kinetics and inverse isotope effect of marine nitrite-oxidizing isolates. Aquat Microb Ecol 80:289–300. https://doi.org/10.3354/ame01859.
15. Kobayashi K, Makabe A, Yano M, Oshiki M, Kindaichi T, Casciotti KL, Okabe S. 2019. Dual nitrogen and oxygen isotope fractionation during anaerobic ammonium oxidation by anammox bacteria. ISME J 13:2426–2436. https://doi.org/10.1038/s41396-019-0440-x.
16. Daims H, Lebedeva EV, Pjevac P, Han P, Herbold C, Albertsen M, Jehmlich N, Palatinszky M, Vierheilig J, Bulaev A, Kirkegaard RH, Von Bergen M, Rattei T, Bendinger B, Nielsen PH, Wagner M. 2015. Complete nitrification by Nitrospira bacteria. Nature 528:504–509. https://doi.org/10.1038/nature16461.
17. Van Kessel MAHJ, Speth DR, Albertsen M, Nielsen PH, Op Den Camp HJM, Kartal B, Jetten MSM, Lücker S. 2015. Complete nitrification by a single microorganism. Nature 528:555–559. https://doi.org/10.1038/nature16459.
18. Pjevac P, Schauberger C, Poghosyan L, Herbold CW, van Kessel MAHJ, Daebeler A, Steinberger M, Jetten MSM, Lücker S, Wagner M, Daims H. 2017. AmoA-targeted polymerase chain reaction primers for the specific detection and quantification of comammox Nitrospira in the environment. Front Microbiol 8:1508. https://doi.org/10.3389/fmicb.2017.01508.
19. Jung MY, Sedlacek CJ, Kits KD, Mueller AJ, Rhee SK, Hink L, Nicol GW, Bayer B, Lehtovirta-Morley L, Wright C, de la Torre JR, Herbold CW, Pjevac P, Daims H, Wagner M. 2021. Ammonia-oxidizing archaea possess a wide range of cellular ammonia affinities. ISME J https://doi.org/10.1038/s41396-021-01064-z.

20. Suzuki I, Dular U, Kwok SC. 1974. Ammonia or ammonium ion as substrate for oxidation by Nitrosomonas europaea cells and extracts. J Bacteriol 120:556–558. https://doi.org/10.1128/jb.120.1.556-558.1974.
21. Kits KD, Sedlacek CJ, Lebedeva EV, Han P, Bulaev A, Pjevac P, Daebeler A, Romano S, Albertsen M, Stein LY, Daims H, Wagner M. 2017. Kinetic analysis of a complete nitrifier reveals an oligotrophic lifestyle. Nature 549:269–272. https://doi.org/10.1038/nature23679.
22. Nowka B, Daims H, Spieck E. 2015. Comparison of oxidation kinetics of nitrite-oxidizing bacteria: nitrite availability as a key factor in niche differentiation. Appl Environ Microbiol 81:745–753. https://doi.org/10.1128/AEM.02734-14.
23. Pester M, Rattei T, Flechl S, Gröngröft A, Richter A, Overmann J, Reinhold-Hurek B, Loy A, Wagner M. 2012. AmoA-based consensus phylogeny of ammonia-oxidizing archaea and deep sequencing of amoA genes from soils of four different geographic regions. Environ Microbiol 14:525–539. https://doi.org/10.1111/j.1462-2920.2011.02666.x.
24. Martens-Habbena W, Berube PM, Urakawa H, De La Torre JR, Stahl DA. 2009. Ammonia oxidation kinetics determine niche separation of nitrifying Archaea and Bacteria. Nature 461:976–979. https://doi.org/10.1038/nature08465.
25. Sakoula D, Koch H, Frank J, Jetten MS, van Kessel MA, Lücker S. 2021. Enrichment and physiological characterization of a novel comammox Nitrospira indicates ammonium inhibition of complete nitrification. ISME J 15:1010–1024. https://doi.org/10.1038/s41396-020-00827-4.
26. Lücker S, Wagner M, Maixner F, Pelletier E, Koch H, Vacherie B, Rattei T, Damsté JSS, Spieck E, Le Paslier D, Daims H. 2010. A Nitrospira metagenome illuminates the physiology and evolution of globally important nitrite-oxidizing bacteria. Proc Natl Acad Sci U S A 107:13479–13484. https://doi.org/10.1073/pnas.1003860107.
27. Mundinger AB, Lawson CE, Jetten MSM, Koch H, Lücker S. 2019. Cultivation and transcriptional analysis of a canonical Nitrospira under stable growth conditions. Front Microbiol 10:1325. https://doi.org/10.3389/fmicb.2019.01325.
28. Daims H, Lücker S, Wagner M. 2016. A new perspective on microbes formerly known as nitrite-oxidizing bacteria. Trends Microbiol 24:699–712. https://doi.org/10.1016/j.tim.2016.05.004.
29. Lücker S, Nowka B, Rattei T, Spieck E, Daims H. 2013. The genome of Nitrospina gracilis illuminates the metabolism and evolution of the major marine nitrite oxidizer. Front Microbiol 4:27. https://doi.org/10.3389/fmicb.2013.00027.
30. Yoshida N. 1988. ^{15}N-depleted N_2O as a product of nitrification. Nature 335:528–529. https://doi.org/10.1038/335528a0.
31. Kritee K, Sigman DM, Granger J, Ward BB, Jayakumar A, Deutsch C. 2012. Reduced isotope fractionation by denitrification under conditions relevant to the ocean. Geochim Cosmochim Acta 92:243–259. https://doi.org/10.1016/j.gca.2012.05.020.
32. Hoch MP, Fogel ML, Kirchman DL. 1992. Isotope fractionation associated with ammonium uptake by a marine bacterium. Limnol Oceanogr 37:1447–1459. https://doi.org/10.4319/lo.1992.37.7.1447.
33. Mooshammer M, Alves RJE, Bayer B, Melcher M, Stieglmeier M, Jochum L, Rittmann SKMR, Watzka M, Schleper C, Herndl GJ, Wanek W. 2020. Nitrogen isotope fractionation during archaeal ammonia oxidation: coupled estimates from measurements of residual ammonium and accumulated nitrite. Front Microbiol 11:1710. https://doi.org/10.3389/fmicb.2020.01710.
34. Liu S, Han P, Hink L, Prosser JI, Wagner M, Brüggemann N. 2017. Abiotic conversion of extracellular NH_2OH contributes to N_2O emission during ammonia oxidation. Environ Sci Technol 51:13122–13132. https://doi.org/10.1021/acs.est.7b02360.
35. Kits KD, Jung MY, Vierheilig J, Pjevac P, Sedlacek CJ, Liu S, Herbold C, Stein LY, Richter A, Wissel H, Brüggemann N, Wagner M, Daims H. 2019. Low yield and abiotic origin of N_2O formed by the complete nitrifier Nitrospira inopinata. Nat Commun 10:1836. https://doi.org/10.1038/s41467-019-09790-x.
36. Daebeler A, Kitzinger K, Koch H, Herbold CW, Steinfeder M, Schwarz J, Zechmeister T, Karst SM, Albertsen M, Nielsen PH, Wagner M, Daims H. 2020. Exploring the upper pH limits of nitrite oxidation: diversity, ecophysiology, and adaptive traits of haloalkalitolerant Nitrospira. ISME J 14:2967–2979. https://doi.org/10.1038/s41396-020-0724-1.
37. Lebedeva EV, Off S, Zumbrägel S, Kruse M, Shagzhina A, Lücker S, Maixner F, Lipski A, Daims H, Spieck E. 2011. Isolation and characterization of a moderately thermophilic nitrite-oxidizing bacterium from a geothermal spring. FEMS Microbiol Ecol 75:195–204. https://doi.org/10.1111/j.1574-6941.2010.01006.x.
38. Widdel F. 1980. Anaerober Abbau von Fettsäuren und Benzoesäure durch neu isolierte Arten Sulfat-reduzierender Bakterien. Georg-August-Universität zu Göttingen, Göttingen, Germany.
39. Hood-Nowotny R, Umana NH-N, Inselbacher E, Oswald-Lachouani P, Wanek W. 2010. Alternative methods for measuring inorganic, organic, and total dissolved nitrogen in soil. Soil Sci Soc Am J 74:1018–1027. https://doi.org/10.2136/sssaj2009.0389.
40. Lachouani P, Frank AH, Wanek W. 2010. A suite of sensitive chemical methods to determine the δ15N of ammonium, nitrate and total dissolved N in soil extracts. Rapid Commun Mass Spectrom 24:3615–3623. https://doi.org/10.1002/rcm.4798.
41. Fry B. 2006. Stable isotope ecology. Springer, New York, NY.
42. R Core Team. 2008. An introduction to dplR. Ind Commer Train 10:11–18.
43. Casciotti KL, McIlvin M, Buchwald C. 2010. Oxygen isotopic exchange and fractionation during bacterial ammonia oxidation. Limnol Oceanogr 55:753–762. https://doi.org/10.4319/lo.2010.55.2.0753.